Paper No. 52

COUPLED ROTOR/AIRFRAME

VIBRATION ANALYSIS

Shmuel Fledel, Omri Rand and Indejit Chopra

Center for Rotorcraft Education and Research

Department of Aerospace Engineering

University of Maryland

College Park, Maryland 20742, U.S.A.

Coupled Rotor/Airframe Vibration Analysis[1]

Shmuel Fledel[2], Omri Rand[3] and Indejit Chopra[4]

Center for Rotorcraft Education and Research

Department of Aerospace Engineering

University of Maryland

College Park, Maryland 20742, U.S.A.

1. Abstract

The paper presents a consistent finite-element formulation, developed for the prediction of vibration in rotor/body helicopter systems in forward flight, taking into account interactional rotor/body loads and dynamic coupling. The rotor and the body are assumed to be elastic beams undergoing transverse, torsion and axial deflections. The coupled analysis is formulated retaining consistently nonlinear terms in the structural, inertial and aerodynamic analysis. Rotor excitation includes rotor/body interactional loads in addition to the fuselage dynamic couplings. Effects of several parameters on vibratory hub loads and body vibration are investigated including blade stiffness, rotor/body clearance, hub location, fuselage stiffness and advance ratio. Significant influence of body upwash on rotor disk in causing vibratory hub shear is shown, which generally increases with smaller rotor/body clearance. By tuning rotor and body natural modes, vibration levels can be substantially reduced.

---

2. Introduction

Vibration in helicopters is a serious problem in helicopter design and operation. At this time, prediction techniques to determine vibration in a helicopter rotor/body system are not reliable. Currently, passive control devices, such as vibration absorbers and isolators are routinely used to reduce vibration at some selected critical points at a considerable weight penalty. Thus, there remains a need to design a helicopter with inherently low vibration. For this, it is essential to develop an analytical formulation which can reliably predict vibration of a rotor/body system under different flight conditions.

The highly nonsteady aerodynamic environment at the rotor disk cause substantial vibratory motion of inherently flexible rotor blades, and in turn, the oscillatory aerodynamic and inertial forces are transmitted to the airframe in the form of hub forces and moments. These , in conjunction with rotor/body interactional aerodynamic forces, are the primary sources of airframe vibration.

The objective of this paper is to calculate the vibration response of a rotor/body system in forward flight using a consistent finite element formulation in space and time, and including rotor/body interactional aerodynamic effects.

In the literature, there have been attempts to predict the vibration of a rotor/body system with a variety of assumptions and solution methods (see recent reviews, Refs. [1] and [2]). For example, in References [3]-[6], impedance matching techniques were used to determine the vibration of a very idealized rigid fuselage, and with a simple rigid rotor model. In Refs. [7] and [8], consistent structural

couplings for a rotor/body system were introduced for a rigid body, together with an elastic rotor. In Ref. [9], the body was assumed to be an elastic beam, but the rotor consisted of rigid blades. However, this work was restricted to hover flight and flap response only.

Reference [10] presents a general purpose comprehensive rotorcraft aerodynamics and dynamics analysis called CAMRAD, which besides many other functions can also predict rotor/fuselage coupled behavior.

Refs. [11] and [12] present a vibration analysis for coupled rotor/fuselage configurations, based on a model of an elastic fuselage. The aerodynamic load predictions were performed using a prescribed wake model, and a panel method was used for calculating the fuselage influence in forward flight. The formulation has been successfully used for predicting the proper trends in vibration levels as functions of the advance ratio.

Existing analysis tools were combined in Ref. [13] where the C81 dynamically coupled rotor/airframe analysis was used to develop rotor hub loads which were used as input to a NASTRAN finite element model of the AH-1G fuselage. Reference [14] models the aeromechanic problems associated with multirotor vehicles where two rotors are connected by a flexible support.

The coupled dynamic response solution is usually based on "rotor/ body iterations" or on "fully coupled" approach. The differences between these methods were discussed in Ref. [15] where it was concluded that both methods are capable of predicting fully coupled behavior.

Most of the existing analyses except Ref. [16], neglect effects of rotor/body interactional aerodynamics in the estimation of body vibration. However, in Ref. [16] the elastic degrees of freedom were

restricted to flap only (i.e. no elastic lag and torsion motions were considered). The solution was based on harmonic representation of the time-dependent variables and modal analysis. In the present paper, the aerodynamic interactional effects on vibration are included by taking into account the fuselage induced velocity distribution over the rotor disk, and the analysis is developed based on nonlinear finite-element modeling of fully coupled elastic rotor and elastic fuselage in a trimmed level flight condition.

3. Analysis

3.1 Blade modeling

The helicopter rotor is assumed to have N_b elastic blades. Each blade is assumed to be an elastic beam undergoing flap bending, lag bending, elastic twist and axial deflection. In the analysis, the blade is discretized into a number of beam elements. Each beam element consists of fifteen degrees of freedom. The finite element formulation is based on Hamilton's principle (Refs. [17] and [18]). The analysis is developed for a blade having pretwist, precone and chordwise offsets of blade center of gravity and aerodynamic center from the elastic axis. Aerodynamic loads are based on a quasisteady strip theory approximation. Noncirculatory loads are also included based on unsteady thin airfoil theory (Ref. [19]). For the steady induced inflow distribution on the rotor disk, the Drees linear inflow model (Ref. [20]), the White and Black linear model (Ref. [21]) and the Vortex Ring model (Ref. [22]) are used.

Hub motion (velocity and acceleration) is included in deriving the

nonlinear blade equations of motion. Rotor-fuselage aerodynamic and dynamic coupling are also included.

The following assumptions have been made :

1. The helicopter is assumed to be in a straight and level forward flight with a constant flight velocity.

2. The blades are cantilevered to the hub.

3. The blade feathering axis is preconed by a constant angle θ_p.

4. The blades have a straight elastic axis.

5. The blades may have distributed built in twist about the undeformed elastic axis.

6. Each blade can bend in two mutually perpendicular directions normal to the elastic axis and can twist torsionally about the elastic axis. Moderate deflections are assumed resulting in small strain and finite rotations.

7. During deformation, the blade cross - sections remain plane and normal to the elastic axis (Bernoulli-Euler hypothesis).

8. Rotor loads are calculated by two - dimensional quasisteady aerodynamic loads. Compressibility and stall effects are neglected.

9. The rotor angular velocity is assumed to be constant (Ω).

10. The rotor shaft is assumed to be rigid.

11. Control system flexibility and engine dynamics are neglected.

3.2 Hub Loads

The hub loads are obtained using a force summation method. Motion induced aerodynamic and inertial loads are integrated along the blade span to obtain blade loads at the root, and then summed over all the blades to obtain the rotor hub loads.

The calculation of the steady (zero harmonic) hub loads are required for trimming the helicopter. The higher harmonic (n>2) components are responsible for helicopter vibration. These consist of three hub forces, longitudinal (F_{xh}), lateral (F_{yh}), and vertical (F_{zh}), and three hub moments, rolling (M_{xh}), pitching (M_{yh}) and yawing (M_{zh}). The blade loads include six components of forces and moments at the blade root; radial (F_{xR}), chordwise (F_{yR}) and vertical (F_{zR}) blade root shear forces, and the torsional (M_{xR}), flapwise (M_{yR}) and lagwise (M_{zR}) blade root moments in the undeformed blade frame. The expressions for motion-induced inertial and aerodynamic loads are described in detail in Refs. [8] and [23].

For the resultant blade loads, the hub-motion-induced inertial loads are added to the aerodynamic and other inertial loads :

$$L = L_u \bar{i} + L_v \bar{j} + L_w \bar{k} = L^A + L^I + L^H$$
$$M = M_u \bar{i} + M_v \bar{j} + M_w \bar{k} = M^A + M^I + M^H \tag{1}$$

Using a force summation method, the nondimensional blade root loads in the undeformed blade frame are given as :

$$F_{xR} = \int_0^1 L_u \, dx$$

$$F_{yR} = \int_0^1 L_v \, dx$$

$$F_{zR} = \int_0^1 L_w \, dx$$

$$M_{xR} = \int_0^1 (M_u - wL_v + vL_w) \, dx \tag{2}$$

$$M_{yR} = \int_0^1 (M_v + wL_u - (x + u)L_w) \, dx$$

$$M_{zR} = \int_0^1 (M_w - wL_u + (x + u)L_v) \, dx$$

Transforming the blade root loads into the hub-fixed nonrotating frame and summing over N_b blades, one obtains the hub loads in the hub fixed nonrotating frame as follows :

$$F_{xh} = \sum_{n=1}^{N_b} (F_{xR}^{(n)}\cos\psi_n - F_{yR}^{(n)}\sin\psi_n - F_{zR}^{(n)}\cos\psi_n\cdot \beta_p)$$

$$F_{yh} = \sum_{n=1}^{N_b} (F_{xR}^{(n)}\sin\psi_n + F_{yR}^{(n)}\cos\psi_n - F_{zR}^{(n)}\sin\psi_n\cdot \beta_p)$$

$$F_{zh} = \sum_{n=1}^{N_b} (F_{xR}^{(n)} \cdot \beta_p + F_{zR}^{(n)})$$

$$M_{xh} = \sum_{n=1}^{N_b} (M_{xR}^{(n)}\cos\psi_n - M_{yR}^{(n)}\sin\psi_n - M_{zR}^{(n)}\cos\psi_n\cdot \beta_p)$$

$$M_{yh} = \sum_{n=1}^{N_b} (M_{xR}^{(n)}\sin\psi_n + M_{yR}^{(n)}\cos\psi_n - M_{zR}^{(n)}\sin\psi_n\cdot \beta_p)$$

$$M_{zh} = \sum_{n=1}^{N_b} (M_{xR}^{(n)} \cdot \beta_p + M_{zR}^{(n)}) \tag{3}$$

where the superscript n denotes the blade number.

The azimuth angle is :

$$\psi_n = \psi_1 + 2\pi(n-1)/N_b \tag{4}$$

Equation (3) may be described as a function of ψ and therefore may be expressed in terms of Fourier series coefficients. For a tracked rotor, where blades are identical structurally and aerodynamically, these expressions contain integer multipliers of N_b/rev. harmonics only.

3.3 Fuselage Modeling

3.3.1 Fuselage Equations of Motion

The fuselage is represented by a flexible beam undergoing vertical bending deflection plus plunging and pitching rigid body degrees of freedom.

The differential equation of motion for the fuselage can be written as :

$$\frac{d^2}{dl^2}\left(EI \; \frac{d^2 z_f}{dl^2} \right) + m\ddot{Z}_f = F_{z_f} \tag{5}$$

where F_{z_f} presents the force acting on the fuselage, including the hub transmitted force, aerodynamic and gravity forces.

The fuselage is discretized into a number of beam elements. Each element consists of four degree of freedom. Natural vibration characteristics are calculated and these are used to obtain normal mode equations for the airframe.

$$\ddot{q}_{i_f} M_{i_f} + v_{i_f}^2 M_{i_f} q_{i_f} = S_{i_f}(t) \tag{6}$$

. where :

$$M_{i_f} = \int_o^l \phi_{i_f}^2(l) \; \bar{m}_f(l) \; dl$$

$$v_i = \frac{\omega_f}{\Omega_{OR}} \tag{7}$$

$$S_{i_f}(t) = \frac{1}{\Omega_{OR}^2 m_o R} \int_o^l \phi_{i_f}(l) \; F_{z_f} \; dl$$

In the present paper, the first and second modes are the rigid body plunging and the rigid body pitching motion respectively while the

higher modes are elastic modes (three elastic modes have been considered).

It is also assumed that the fuselage is excited by the N_b/rev. hub vertical force and hub pitching moment, plus interactional aerodynamic forces distributed along the length of the beam. It is assumed that the fuselage steady response is periodic in N_b/rev.

The hub reaction at $l = x_h$, $Z_f(x_h, t)$ may therefore be described by the nondimentional time (or azimuth angle) ψ :

$$Z_h(\psi) = Z_f(x_h, \psi) = \sum_{i=1}^{n} \phi_{i_f}(x_h) q_{i_f}(\psi)$$

$$\dot{Z}_h(\psi) = \dot{Z}_f(x_h, \psi) = \sum_{i=1}^{n} \phi_{i_f}(x_h) \dot{q}_{i_f}(\psi) \qquad (8)$$

$$\ddot{Z}_h(\psi) = \ddot{Z}_f(x_h, \psi) = \sum_{i=1}^{n} \phi_{i_f}(x_h) \ddot{q}_{i_f}(\psi)$$

Based on the above mentioned assumptions S_{i_f}, $q_{i_{j_f}}$ and their derivatives may be written as :

$$S_{i_f} = S_0 + S_{c_i} \cos(jN_b\psi) + S_{s_i} \sin(jN_b\psi) \qquad (9)$$

$$q_{i_{j_f}} = q_{0_i} + q_{c_{ij}} \cos(jN_b\psi) + q_{s_{ij}} \sin(jN_b\psi)$$

$$\dot{q}_{i_{j_f}} = (jN_b) \left[- q_{c_{ij}} \sin(jN_b\psi) + q_{s_{ij}} \cos(jN_b\psi) \right] \qquad (10)$$

$$\ddot{q}_{i_{j_f}} = -(jN_b)^2 \left[q_{c_{ij}} \cos(jN_b\psi) + q_{s_{ij}} \sin(jN_b\psi) \right]$$

Solving the differential equation (6) yields :

$$q_{0_i} = \frac{S_{0_i}}{M_{i_f} v_{i_f}^2} \qquad i=3,4...$$

$$q_{c_{ij}} = \frac{S_{c_{ij}}}{M_{i_f} \left[v_{i_f}^2 - (jN_b)^2 \right]} \qquad i=1,2... \qquad (11)$$

$$q_{s_{ij}} = \frac{S_{s_{ij}}}{M_{i_f} \left[v_{i_f}^2 - (jN_b)^2 \right]} \qquad i=1,2...$$

Note that $q_{0_1} = q_{0_2} = 0$ as a result of trim considerations. Note :

$$Z_f(l,t) = \sum_{i=1}^{N} \phi_{i_f}(l) \; q_i(t) \tag{12}$$

and using Eqs. (9)-(10), one gets the fuselage displacement, velocity and acceleration at any point.

3.3.2 Fuselage Aerodynamic Model

The fuselage aerodynamic model and its upwash effect on the main rotor is based on the model described in Ref. [24]

The fuselage shapes are obtained by a distribution of discrete sources/sinks along its axis which, together with the freestream velocity, create bodies with two planes of symmetry. This method enables one describe a large family of helicopter-like shapes with a few sources and sinks.

The fuselage shape is determined by the case of an isolated fuselage at a zero yaw angle. The stream function ψ_f due to a uniform freestream velocity V in the x direction and the distribution of n discrete sources G_i at point x_i along the fuselage axis can be formulated in the x-z plane as:

$$\psi_f = - \; \tilde{z}^2 + \frac{1}{2} \sum_{i=1}^{n} \bar{G}_i \frac{\tilde{x} - \tilde{x}_i}{\sqrt{(\tilde{x} - \tilde{x}_i)^2 + \tilde{z}^2}} \tag{13}$$

where $(\tilde{\;})$ and $(\bar{\;})$ represent nondimensionalizations by the disk radius R and $\pi V R^2$, respectively.

The fuselage reaction in terms of its upwash due to the rotor downwash is derived by distributing additional sources over the fuselage surface (see also Ref. [16]).

3.4 Solution Procedure

The present solution is based on a coupled analysis where trim parameters and rotor fuselage response parameters are calculated from a coupled set of equations.

To start the process, an uncoupled vehicle trim solution is calculated. This uncoupled trim solution is needed as an initial guess for the complete coupled trim and response analysis (Ref. [25]). In the present paper, the propulsive trim is used. Hub loads are calculated using a force summation method (see section 3.2).

The finite element method in time is used to determine periodic deflections for the fuselage and the blade. The time period of one rotor revolution is discretized into a number of time elements. To reduce computation time, blade finite element equations in the space-domain are transformed into the modal domain using the coupled natural modes.

The complete coupled solution is calculated using a nonlinear solver (IMSL-ZSPOW, Ref. [26]). The key simplification achieved by using this method is the ability of being able to put all structural nonlinear terms, all aerodynamic forces and the coupling terms to the right hand side of the fully coupled set of equations in their explicit form. The analytical effort is therefore drastically minimized. The method enables the user to include additional nonlinear aerodynamic or structural terms of the equation with no extra effort.

3.4.1 Finite Element Method In Time Procedure

The finite element formulation is based on Hamilton's principle in weak form which may be formulated as :

$$\delta\Pi = \int_{t_1}^{t_2} (\ \delta U - \delta T - \delta W \ ) = 0 \tag{14}$$

where $\delta U, \delta T$ and δW are the variation of strain energy, kinetic energy and the virtual work done by external forces. Substitution of suitable expressions for $\delta U, \delta T$ and δW in Hamilton's principle would result in the equations of motion. Detailed expressions for $\delta U, \delta T$ have been derived in Ref.[8] and [18].

From Hamilton's principle Eq. (14), the following integral expression is obtained (see Ref. [27]) :

$$\int_{\psi_I}^{\psi_F} \delta q^T (\ M\ddot{q} + C\dot{q} + Kq - F \ ) \, d\psi = 0 \tag{15}$$

The associated matrices , $i.e.$, the global mass M, damping C, stiffness K and force vector F in the space domain, contain periodic terms. For convenience, all the nonlinear terms are put in the force vector. Integrating this equation by part and rearranging, gives the following equation in the reduced form :

$$\int_{\psi_I}^{\psi_F} \delta Y^T \ Q \, d\psi = \delta Y^T \ B \tag{16}$$

where :

$$Y = \left\{ \begin{matrix} q \\ \dot{q} \end{matrix} \right\}$$

$$Q = \left\{ \begin{matrix} F - C\dot{q} - Kq \\ M\dot{q} \end{matrix} \right\}$$

$$B = \left\{ \begin{matrix} M\dot{q} \\ 0 \end{matrix} \right\}_{\psi_I}^{\psi_F} \tag{17}$$

and the ψ_I and ψ_F represent the initial and final state of time, and B is a boundary term. For the periodic response solution, one may choose :

$$\psi_F = \psi_I + T \tag{18}$$

where T is the nondimentional time period of one rotor revolution (i.e.,2π). Thus, the right hand side of Eq. (16) vanishes. Thus,

$$\int_{\psi_I}^{\psi_F} \delta Y^T Q \, d\psi = 0 \tag{19}$$

For N_e time elements, Eq. (19) may be written in a discretized form as :

$$\sum_{i=1}^{N_e} \int_{\psi_i}^{\psi_{i+1}} \delta Y^T Q \, d\psi = 0 \tag{20}$$

where the ψ_i and ψ_{i+1} represent lower and upper time limits for the ith time element.

To reduce computation time, quantities in the space domain are transformed into the modal domain using the coupled natural vibration characteristics. Eq. (20) may be written as :

$$\sum_{i=1}^{N_e} \int_{\psi_I}^{\psi_{I+1}} \delta X_i^T \{ N^T \; \Psi^T \; Q \} \; d\psi = 0 \tag{21}$$

The periodic boundary conditions are enforced for rotor steady response as :

$$X \; (\psi_I = 0) = X \; (\psi_F = T = 2\pi) \tag{22}$$

3.4.2 Coupled Rotor Fuselage

The fuselage equation (6) and rotor equation (21) are coupled. There are two approaches to formulate the couplings :

a). Complete Coupled Formulation :

In this case, all the linear terms of the rotor and fuselage equations are transferred from the right hand side to the left hand side.

$$\begin{bmatrix} M_R & M_{Rf} \\ M_{fR} & M_f \end{bmatrix} \begin{Bmatrix} \ddot{q}_R \\ \ddot{q}_f \end{Bmatrix} + \begin{bmatrix} C_R & C_{Rf} \\ C_{fR} & C_f \end{bmatrix} \begin{Bmatrix} \dot{q}_R \\ \dot{q}_f \end{Bmatrix} + \begin{bmatrix} K_R & K_{Rf} \\ K_{fR} & K_f \end{bmatrix} \begin{Bmatrix} q_R \\ q_f \end{Bmatrix} = \begin{Bmatrix} F_R \\ F_f \end{Bmatrix} \tag{23}$$

In this approach one can get direct evaluation of the eigenvalues and eigenvectors of the system. However, this way suffers from inflexibility in changing any of the terms. It requires linearization of the force terms which lead to additional assumptions and approximations. It is also expected to create a large system of equations which has to be solved simultaneously.

b). Explicit Coupled Formulation :

The second approach is based on an advanced technique for solving nonlinear sets of equations. The rotor/body coupled system of equations are formulated in the following explicit form :

Rotor :

$$[M_R]\{\ddot{q}_R\} + [C_R]\{\dot{q}_R\} + [K_R]\{q_R\} = \left\{F_R\left(\ddot{q}_R, \dot{q}_R, q_R, \ddot{q}_f, \dot{q}_f, q_f\right)\right\}$$

Fuselage :

$$[M_f]\{\ddot{q}_f\} + [C_f]\{\dot{q}_f\} + [K_f]\{q_f\} = \left\{F_f\left(\ddot{q}_R, \dot{q}_R, q_R, \ddot{q}_f, \dot{q}_f, q_f\right)\right\}$$

(24)

Here the rotor/fuselage coupling terms lie on the right hand side with external forces. Therefor the right hand terms are function of the rotor as well as fuselage motion. Rotor and fuselage equations are solved iteratively.

First the solution starts with some assumed vector $\{q_R\}$, and then it is updated internally in the nonlinear solver routine to get the desired $\{q_R\}$ and $\{q_f\}$ vectors. The converged solution represents a fully coupled system.

The main advantage of this kind of solution is the flexibility in changing the fuselage modeling. One doesn't has to make any further assumptions in the ordering of force terms.

It is possible to identify the coupling terms in the forcing expression. However, direct evaluation of the coupled system eigenvalues and eigenvectors has to be done only by frequency sweep in this case.

In the present paper, the second approach is adopted and implemented by a nonlinear solver which is based on variation of Newton's method (see Ref. [26]).

4. Results and Discussion

For numerical results, a typical 4-blade soft inplane hingeless rotor is selected as a baseline configuration. It consists of Lock number $\gamma=5.5$, solidity ratio $\sigma=0.07$, blade aspect ratio $c/R=0.055$, zero precone and zero pretwist. The chordwise offset of blade center of gravity, aerodynamic center, and tensile axis from the elastic axis (e_g, e_d, and e_A), are assumed to be zero. The fuselage center of gravity lies on the shaft axis ($X_{cg}=Y_{cg}=0$), and is located at a distance of $0.3R$ below the rotor hub center. The fuselage drag coefficient in terms of flat plate area ($f/\pi R^2$) is taken as 0.01. The airfoil characteristics used are $C_l=2\pi\alpha$, $C_d=0.01$, $C_m=0.$. For the baseline configuration, the structural properties of the blade and the fuselage are assumed uniform and given in table 1. The analysis is carried out at an advance ratio $\mu=0.3$.

Table 1 - Baseline Properties

R o t o r :

$EI_y/m_0\Omega^2R^4$	0.01000
$EI_z/m_0\Omega^2R^4$	0.02680
$GJ/m_0\Omega^2R^4$	0.00615
k_A/R	0.0290
k_{m_1}/R	0.0132
k_{m_2}/R	0.0247

The first flap, lag, and torsion frequencies are 1.13/rev., 0.70/rev.,

and 4.47/rev., respectively.

Fuselage :

$$EI_y/m_o\Omega^2R^4 \qquad 0.01000$$

The first three elastic natural frequencies are: 1.61/rev., 4.44/rev., 8.71/rev.

A parametric study has been carried out for this baseline configuration. In the following examples, the coupled rotor/fuselage vibration is presented by the N_b/rev. vertical hub force amplitude (is nondimensionalized with respect to $m_o\Omega^2R^2$).

For the analysis, the blade is discretized into six beam elements of equal length, and each beam element consists of 15 nodal degrees of freedom. For the periodic steady response of the rotor, one cycle of time is discretized into six time elements and each time element is discretized by a fifth order Lagrange polynomial distribution along the azimuth. For response calculations, six rotating natural modes which respectively represent three flap, two lag and one torsion mode were used.

Figure 1 shows the baseline rotor/body configuration and Figure 2 shows the finite element discretization. Figure 3 presents the steady tip response obtained using the coupled trim analysis for a thrust level C_T/σ of .07. Lag and torsion responses primarily consist of 1/rev. variation, whereas flap bending response involves 2/rev. variation. The fuselage effect can be easily seen in the variation between the line presenting the response with no fuselage upwash and the other lines that include the fuselage upwash. The response results

with no fuselage upwash however includes in it noncirculatory terms).
For this case the effect of the dynamic coupling (without aerodynamic
interference) was also explored. Its effect on blade response was seen
to be small. As expected, noncirculatory aerodynamic forces are
important for torsional response. Figure 4 shows the fuselage response
in terms of g's (the acceleration $\ddot{Z}_f$ normalized by the
gravity acceleration) at different azimuth locations. Since it is a
four blade rotor, the results in the other three quadrants, i.e. 90^0
to 360^0 are identical. Note that $\ddot{Z}_f$ represents the
resultant vibration amplitude in terms of 'g' acceleration. From the
figure, one can find the vibration level at different stations.

Figures 5 to 15 present the parametric studies to show the
influence of of the major parameters on the body vibration. Note that
for a given hub location, there is direct correlation between the
4/rev. hub transmitted force and the 4/rev. acceleration amplitude.
Consequently, in the following examples results are represented in
terms of the 4/rev. hub force.

Figure 5 shows the rotor/body clearance effect. It can be seen
that the interactional effect becomes larger as the clearance between
rotor and body becomes smaller. Clearly, the normalized hub force
increases sharply due to a large increase in upwash on the rotor disk
as the rotor/body clearance decreases. The change in the controls
setting due to this effect can be seen in Figure 6. There is a small
effect of rotor/fuselage clearance on θ_0 , θ_{ls} , and vehicle
attitude (α_s and ϕ_s). However, θ_{lc} is more affected.

In fig. 7 the sensitivity of the longitudinal hub location on the
fuselage vibratory response is investigated. In this case, the 4/rev.
vertical hub force and the acceleration at body nose (point 1) are

presented. Since the hub location is changed, there is no direct correlation between hub force and acceleration at a body station. The reason for that is explained in Figure 8 where it can be seen that the dominant mode in the fuselage bending and acceleration moves from the 4th (anti-symmetric) mode to the 3rd (symmetric) mode as the hub location point moves towards the center of the fuselage (.9R line). This trend is a result of the uniform distribution of the fuselage properties. The vibration level at body nose becomes smaller as the hub location is moved away from the nose until it reaches 40% of body length then it starts increasing. It is interesting to note that the vertical hub force is minimum when hub located about 25% of body length from nose.

In Figures 9 - 12 the characteristics of the fuselage upwash are studied. Figure 9 shows a sharp monotonic upwash increase as the rotor fuselage clearance decreases at a representative point on the rotor disk at $\psi=180^0$ and $x=0.8$. Figure 10 presents the Fourier coefficients of the upwash at this point. It shows a large 1/rev. component of the upwash, this explains the reason for change in cyclic pitch θ_{lc} as rotor/body clearance changes (Figure 6). The magnitude of harmonics in upwash decrease with higher harmonics. The purpose of Figure 11 is to show the relative magnitude of upwash harmonics in terms of steady value. In this figure the normalized Fourier coefficients for rotor/fuselage clearances h/R=0.2 and h/R=0.5 are presented. Note that the curves are normalized differently. It is interesting to note that relative magnitude of lower harmonics is higher for larger rotor/body clearance whereas it is larger for higher harmonics for smaller clearance. Later on this phenomenon will explain the cause of higher harmonic excitation for cases where the rotor and

the body clearance becomes smaller. Figure 12 shows the values of the fuselage upwash at various radial locations on the rotor disk. There is an upwash on the fore and a downwash on the aft parts of the rotor disk due to body influence. For outboard part of the blade (r/R>.4) the upwash peak is felt at $\psi=180^o$. Also, the maximum upwash occurs about 70% radial position.

Figure 13 shows the effect of the advance ratio μ on the hub force. It is presented for two cases. Case I represents an isolated rotor ($h/R\rightarrow\infty$), and therefore there is no upwash on the disk. In case II, the h/R is 0.3, and there is an upwash field on the disk. It increases oscillatory hub forces. As expected, for both cases, an increase in the 4/rev. hub forces occurs as μ grows.

In Figure 14 the 4/rev. vertical hub force presented with changing rotor stiffness and for different rotor fuselage clearances. As the clearance decreases, sharp peaks start appearing in the 4/rev. hub force, for h/R values below 0.3. These sharp peaks occur for values of rotor stiffness where the natural rotor frequencies, mainly the second flap, are excited by the fuselage upwash higher harmonics (the 3/rev. and 4/rev. - see Figures. 10 and 11) and due to nonlinear effects in the system. For stiffer rotors, increasing rotor/body clearance deteriorates vibratory hub force, whereas for softer rotors larger clearance helps to reduce vertical hub force.

In Figure 15 the effect of the fuselage stiffness on oscillatory hub force is presented. The sharp peak of hub force occurs when the fourth natural body mode and second flap mode coincide with 4/rev. The magnitude of vibratory force changes with changing body stiffness. This shows that by tuning the body natural modes, vibration response can be controlled.

5. Conclusions

A consistent finite element formulation capable of predicting the vibration of rotor/body systems in forward flight has been presented. Both the rotor and the fuselage models are fully elastic and aerodynamic interaction are also included. Parametric investigation of the influence of the critical system's parameters has been carried out.

The model is based on a unique method of solution employing nonlinear numerical solver which enables the inclusion of any nonlinear terms with minimal analytic effort.

The results show a considerable effect of the fuselage (both aerodynamic and dynamic) on the coupled vibratory response. While the most important parameters appear to be the rotor/fuselage clearance and the fuselage stiffness. In particular, it is shown that as the rotor/body clearance is reduced, the vibratory hub loads dramatically increase, which also requires significant changes in trim. In addition , the influence of the advance ratio appears to contribute significantly to vibration. As expected, rotor and fuselage stiffnesses play an important role as well. The results present critical combination of the rotor and fuselage stiffnesses which should be avoided in order to keep low vibration level.

List Of Symbols

a	Blade lift curve slope
A	Rotor disk area
B	Boundary term
c	Blade chord
c_d	Blade section drag coefficient
c_l	Blade section lift coefficient
$c_{m_{ac}}$	Blade section moment coefficient about aerodynamic center
C	Damping matrix
c_T	Thrust coefficient
c_w	Weight coefficient
c_{m_x}	Rolling moment coefficient
c_{m_y}	Pitching moment coefficient
D	Aerodynamic drag per unit of blade length
D_R	Aerodynamic radial drag per unit of blade length
e_A	Chordwise offset of tensile axis from the elastic axis (positive forward)
e_g	Chordwise offset of blade c.g. from elastic axis (positive forward)
e_d	Chordwise offset of aerodynamic center from elastic axis (positive forward)
E	Young's Modulus
EI_y	Blade flap bending stiffness
EI_z	Blade lag bending stiffness
f	Equivalent flat-plate drag area of helicopter
F	Global force vector
g	Gravity acceleration

F	Global force vector
g	Gravity acceleration
G	Shear Modulus
GJ	Blade torsional stiffness
h	Vertical distance of hub center from the helicopter c.g.
H	Longitudinal drag force on the rotor in flight condition
$H(\xi)$	Shape function
I	Identity matrix
K	Global stiffness matrix
M	Global mass matrix
m_0	Reference mass per unit length
N	Shape function for time element
N_b	Number of blades
N_e	Number of time elements
p	Normal mode coordinates
Q	State variables of load vector
q	Blade global coordinates
R	Rotor blade radius
T	Time period of one rotor revolution (2π)
T	Coordinate transformation matrix, Thrust
$\bar{V}$	Vehicle forward velocity
W	Helicopter weight
X	State variable of normal mode coordinates
Y	State variable of blade response
α	Blade section angle of attack
α_s	Longitudinal tilt of shaft
β_p	Blade precone angle
σ	Solidity ratio, $N_b c / \pi R$

Φ	Free vibration eigenvectors
ϕ_s	Lateral tilt of shaft
Ψ	Modal transformation matrix
ψ	Azimuth angle, Ωt
θ_{75}	Collective pitch angle at 75% blade span
θ_{lc}	Lateral cyclic pitch angle
θ_{ls}	Longitudinal cyclic pitch angle
θ_{tw}	Blade linear elastic twist
λ	Rotor inflow ratio
Ω	Rotor speed
ω	Free vibration rotating frequency
γ	Lock Number
μ	Advance ratio

Superscripts and Subscripts

ac	Aerodynamic center
A	related to aerodynamic force
h	Related to hub
f	Related to fuselage
p	Per rev.
R	Related to rotor

References

1. Friedmann, P.P., "Recent Developments in Rotery-Wing Aeroelasticity" Journal of Aircraft, Vol. 14, No. 11, November 1977, pp. 1027-1041.

2. Friedmann, P.P., "Formulation and Solutions of Rotary-Wing Aeroelastic Stability and Response Problems" Vertica, Vol. 7, No. 2, pp. 101-104, 1983.

3. Hohnemeser, K.H. and Yin, S.K., "The Role of Rotor Impedance in the Vibration Analysis of Rotorcraft" Vertica, Vol. 3. 1979, pp.187-204.

4. Hsu, T.K. and Peters, D.A., "Coupled Rotor/Airframe Vibration Analysis by a Combined Harmonic-Balance Impedance Matching Method" 36th AHS forum, May 1980.

5. Kunz, D.L., "A Nonlinear Response Analysis for Coupled Rotor - Fuselage System" AHS Specialists Meeting on Helicopter Vibration, Technology for the Jet Smooth Ride, Nov. 1981.

6. Gabel, R. and Sankewitch, V., "Rotor-Fuselage Coupling by Impedance" AHS 42nd Annual Forum, June 1986.

7. Warmbrot, W. and Friedmann, P.P., "Formulation of Coupled Rotor - Fuselage Equations of Motion" Vertica, Vol. 3, 1979, pp. 245-271.

8. Bir, G. and Chopra, I., "Prediction of Blade Stresses due to Gust Loading" Vertica Vol. 10. 3/4 1986 pp.353-377.

9. Rutkowski, M.J., 'The Vibration Characteristics of Coupled Rotor Fuselage by a Finite Element Analysis" NASA T.P. 2118 Jan. 1980.

10. Johnson, W., "A Comprehensive Analytical Model of Rotorcraft Aerodynamics and Dynamics, Part I: Analysis Development" NASA TM-81182, June 1980.

11. Shoper, R. and Kottapalli, S.B.R., "Correlation of Predicted Vibrations and Test Data for a Wind Tunnel Helicopter Model" AHS 38th Annual Forum May 1982.

12. Shoper, R. and Studwell, R.E., "Coupled Rotor/Airframe Vibration Analysis" NASA CR-3582, 1982.

13. Dompka, R.V. and Corrigan, J.J, "AH-1G Flight Vibration Correlation Using NASTRAN and C81 Rotor/Airframe Coupled Analysis" AHS 42nd Annual Forum June 1986.

14. Venkatesan, C. and Friedmann P.P., "Aeroelastic Effects in Multirotor Vehicles with Application to Hybrid Heavy Lift System, Part I: Formulation of equations of motion" NASA CR-3822, Aug. 1984.

15. Stephens, W.B. and Peters, D.A., "Rotor-Body Coupling Revisited" Journal of the American Helicopter Society, Vol. 32, No. 1, January 1987.

16. Rand, O., "The Influence of Interactional Aerodynamics in Rotor/ Fuselage Coupled Response" 2nd International Conference on Rotorcraft Basic Research, College Park, MD, Feb. 1988.

17. Sivaneri, N.T. and Chopra, I., "Dynamic Stability of Rotor Blade Using Finite Element Analysis" AIAA Journal, Vol.29, No.2, April 1984, pp. 42-51.

18. Panda, B. and Chopra, I., "Flap-Lag-Torsion Stability in Forward Flight" Journal of the American Helicopter Society, Vol. 12A, No. 1, January 1986, pp. 111-130.

19. Fung, Y.C., "An Introduction to the Theory of Aeroelasticity" Dover Publications Inc. N.Y., 1969.

20. Drees, J.M., "A Theory of Airflow Through Rotors and its Application to Some Helicopter Problems" Journal of the Helicopter Association of Great Britain, 3:2 July-September 1949.

21. White, F. and Black, B.B., "Improved Method of Predicting Helicopter Control Response and Gust Sensitivity" AHS 35th Annual Forum May 1979.

22. Harry, H.H and Katoff, S., "Induced Velocities Near a Lifting Rotor with Nonuniform Disk Loading" National Advisory Committee for Aeronautics, Report 1319, 1957.

23. Lim, J.W. and Chopra, I., "Aeroelastic Optimization of Helicopter Rotor" Journal of the American Helicopter Society, Vol. 34, No. 1, January 1989.

24. Rand, O. and Gessow, A., "Model for Investigation of Helicopter Fuselage Influence on Rotor Flowfields" J. Aircraft, Vol.26, No.5, May 1989.

25. Lim, J.W., "Aeroelastic Optimization of Helicopter Rotor" Ph.D. Dissertation, Dept. of Aerospace Engineering, Unversity of Maryland, May 1988.

26. IMSL Library Reference Manual (9.2 edn.). IMSL, Huston, Tex. IMSL LIB - 0009, Nov. 1984.

27. Dull, A.L. and Chopra, I., " Aeroelastic Stability of Bearingless Rotors in Forward Flight" Journal of the American Helicopter Society, Vol. 33, No. 4, October 1988, pp. 38-46.
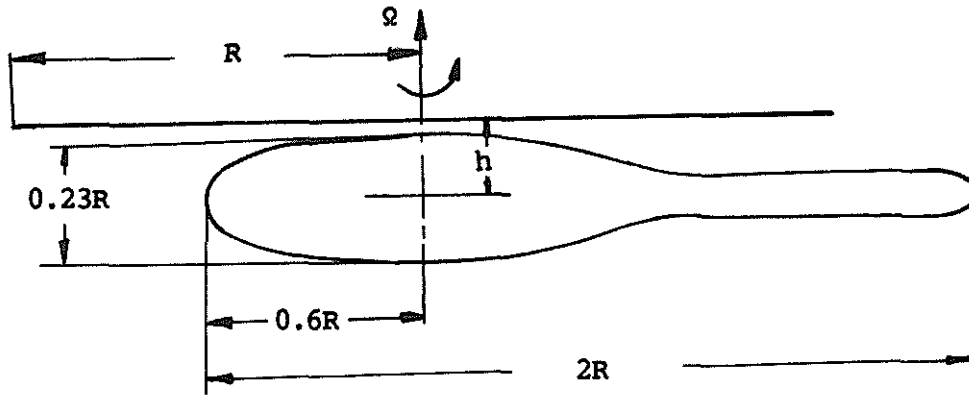
Fig. 1 - Baseline configuration
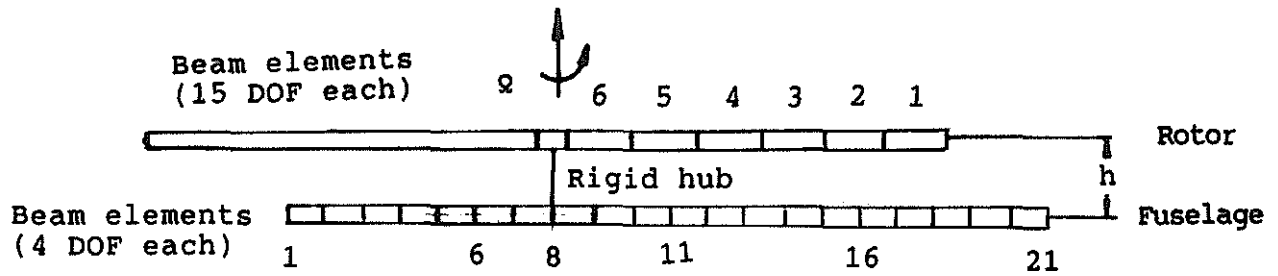
Fig. 2 - Finite element discretization
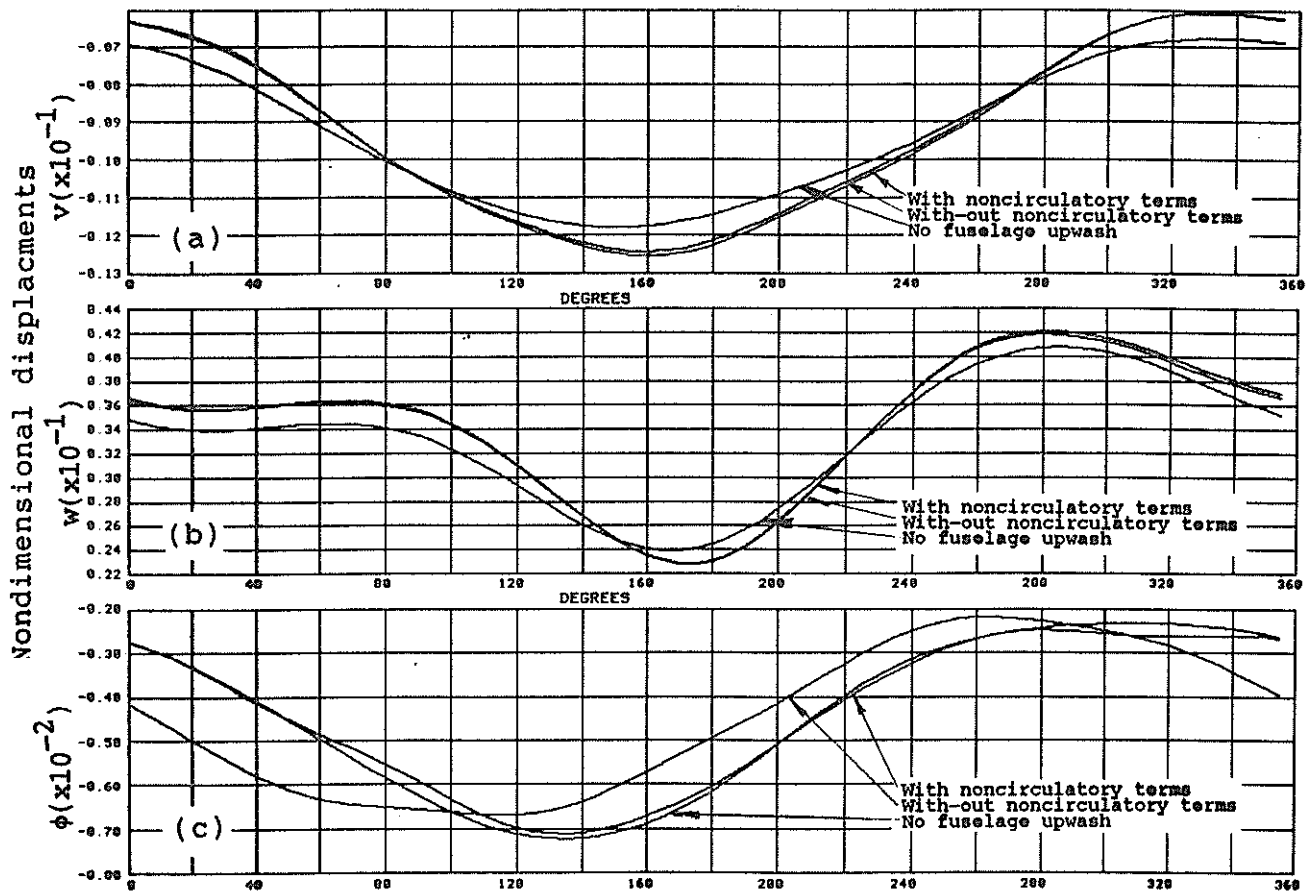
Fig. 3 – Steady tip response – baseline configuration for $\mu=.3$ Ψ(deg.)
(a) Lag   (b) Flap   (c) Torsion
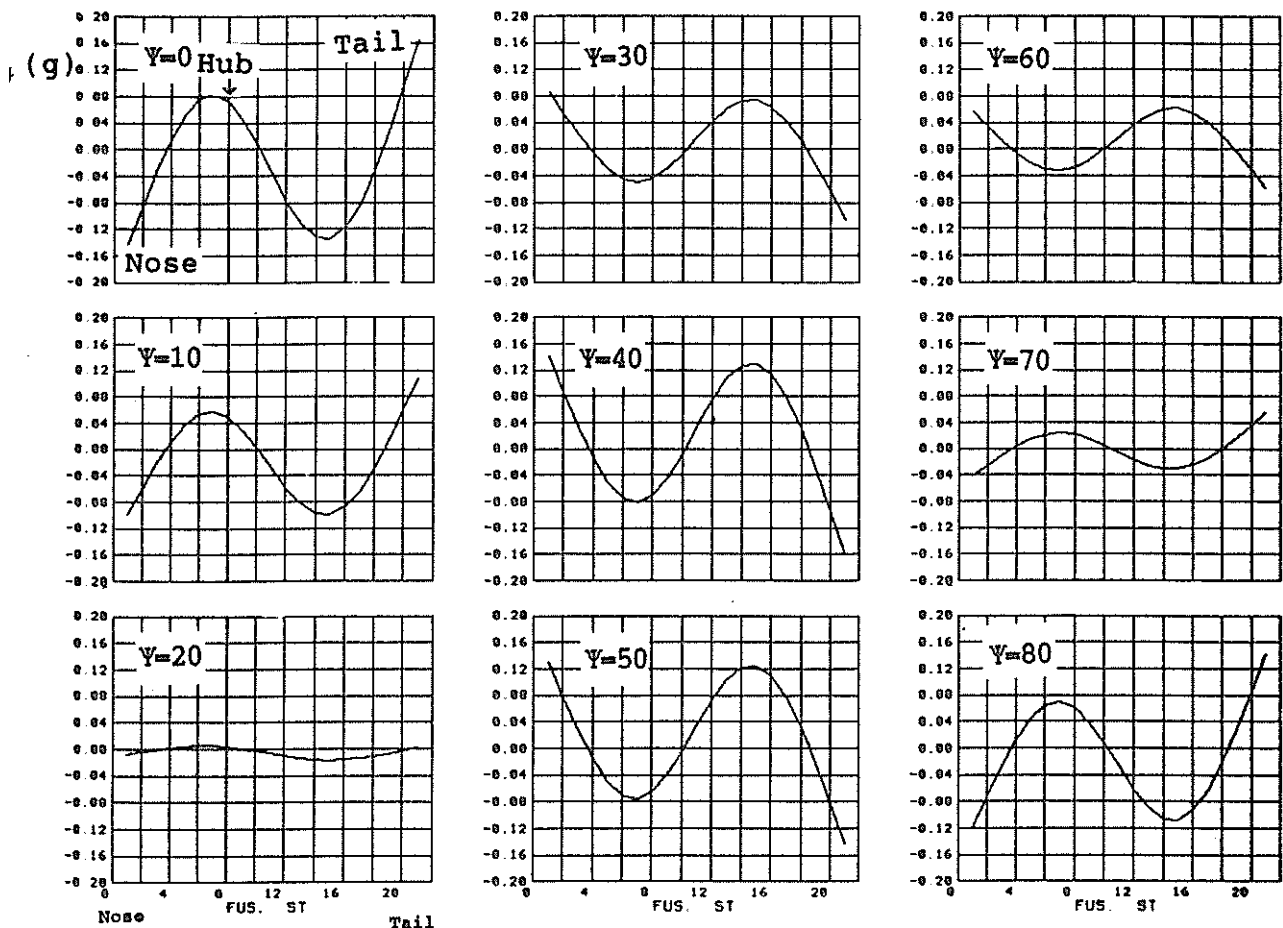
Fig. 4 – Fuselage response – baseline configuration ($\mu=.3$)
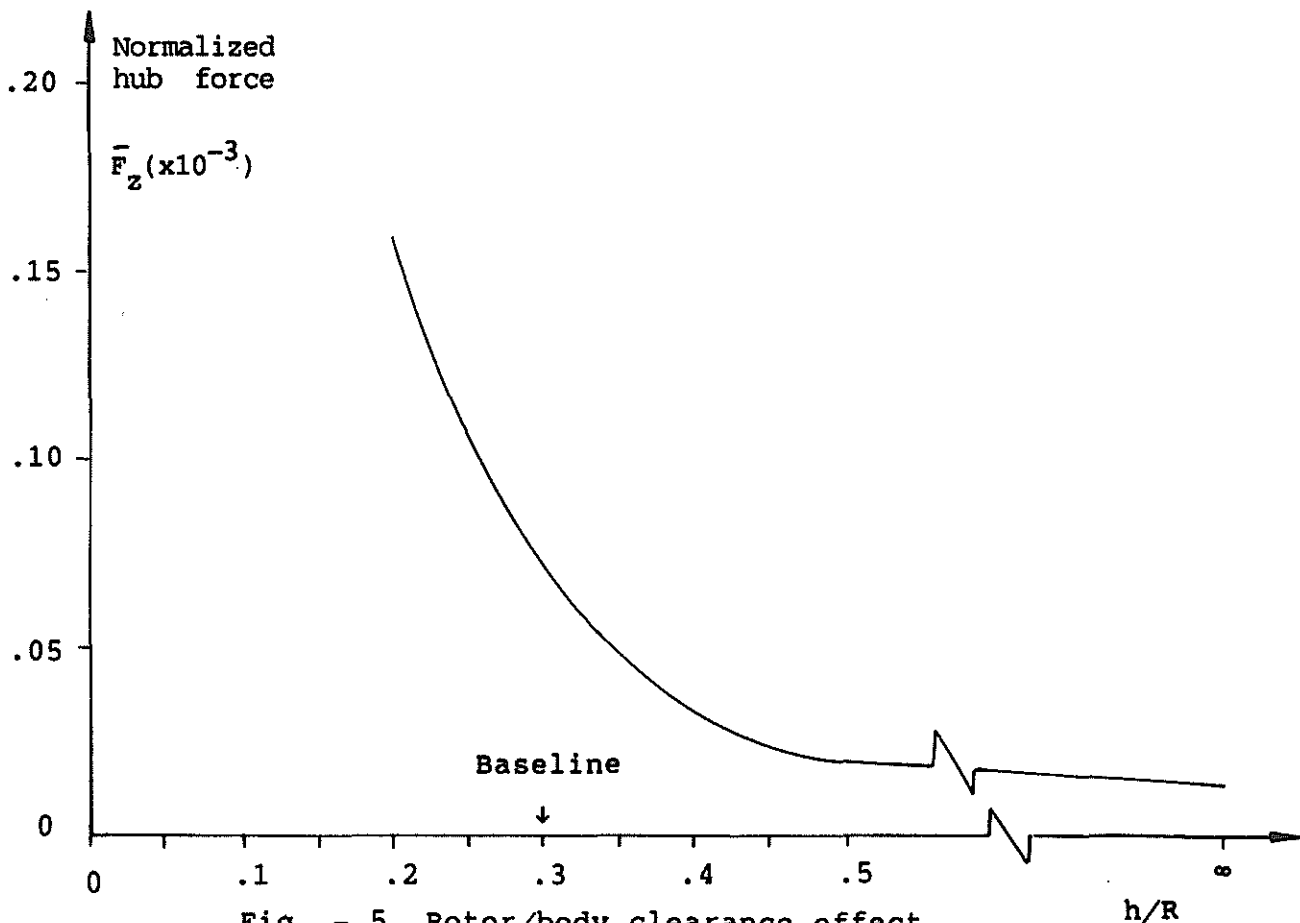
Fig. — 5   Rotor/body clearance effect
on normalized hub force
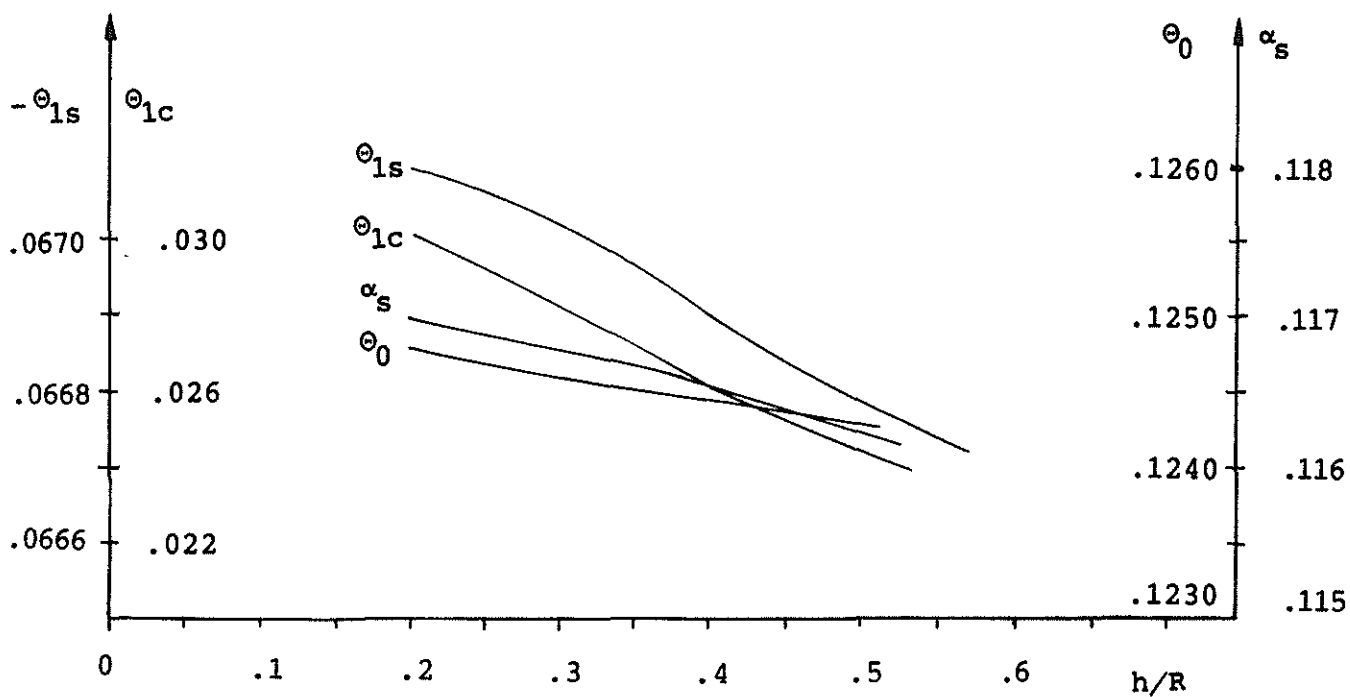
Fig. 6 — Rotor/body   clearance   effect   on
pitch controls and shaft tilt angles
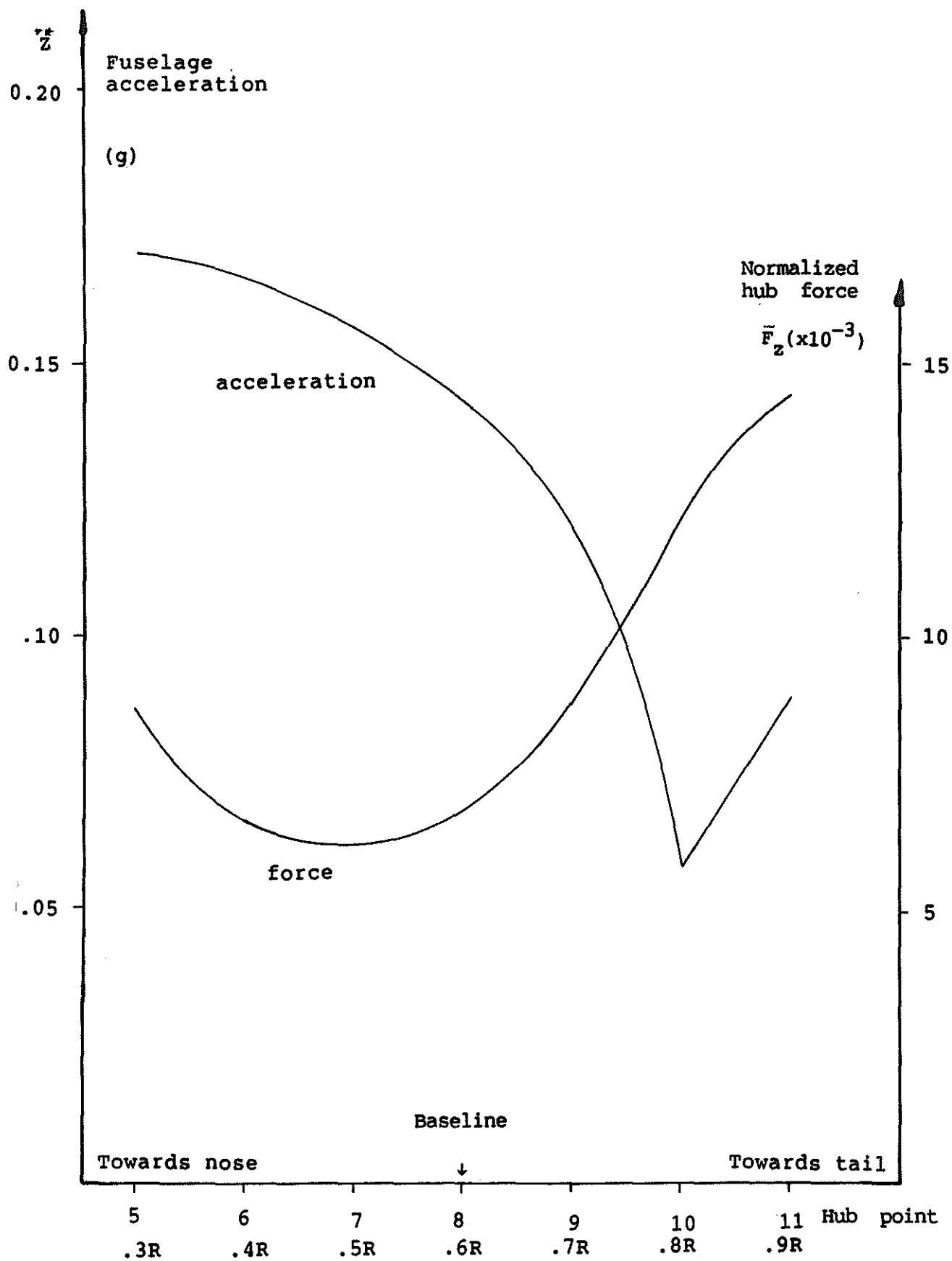
Fig. 7 – Effect of hub location on normalized hub force and fuselage acceleration at nose
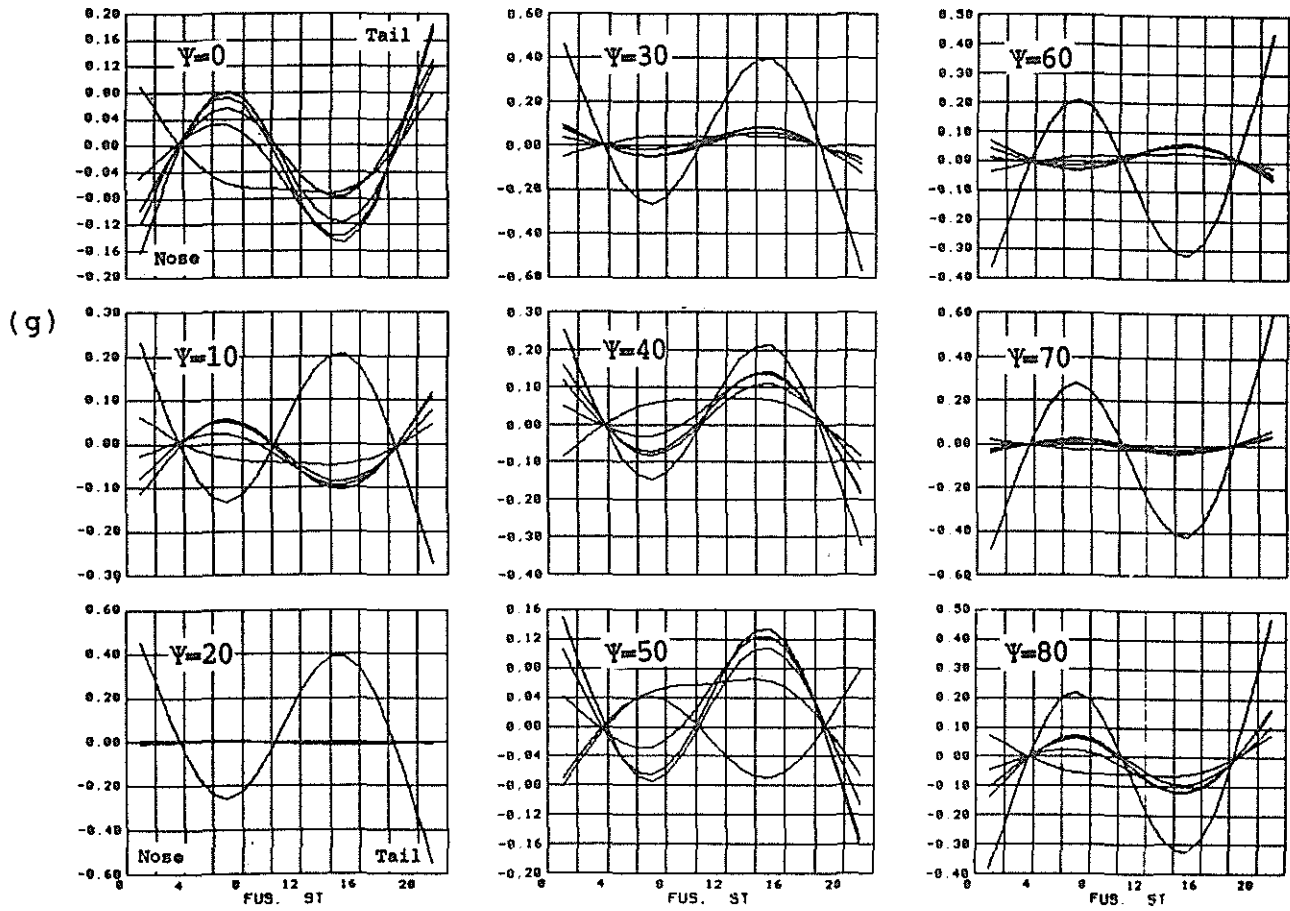
Fig. 8a – Fuselage response at different hub locations
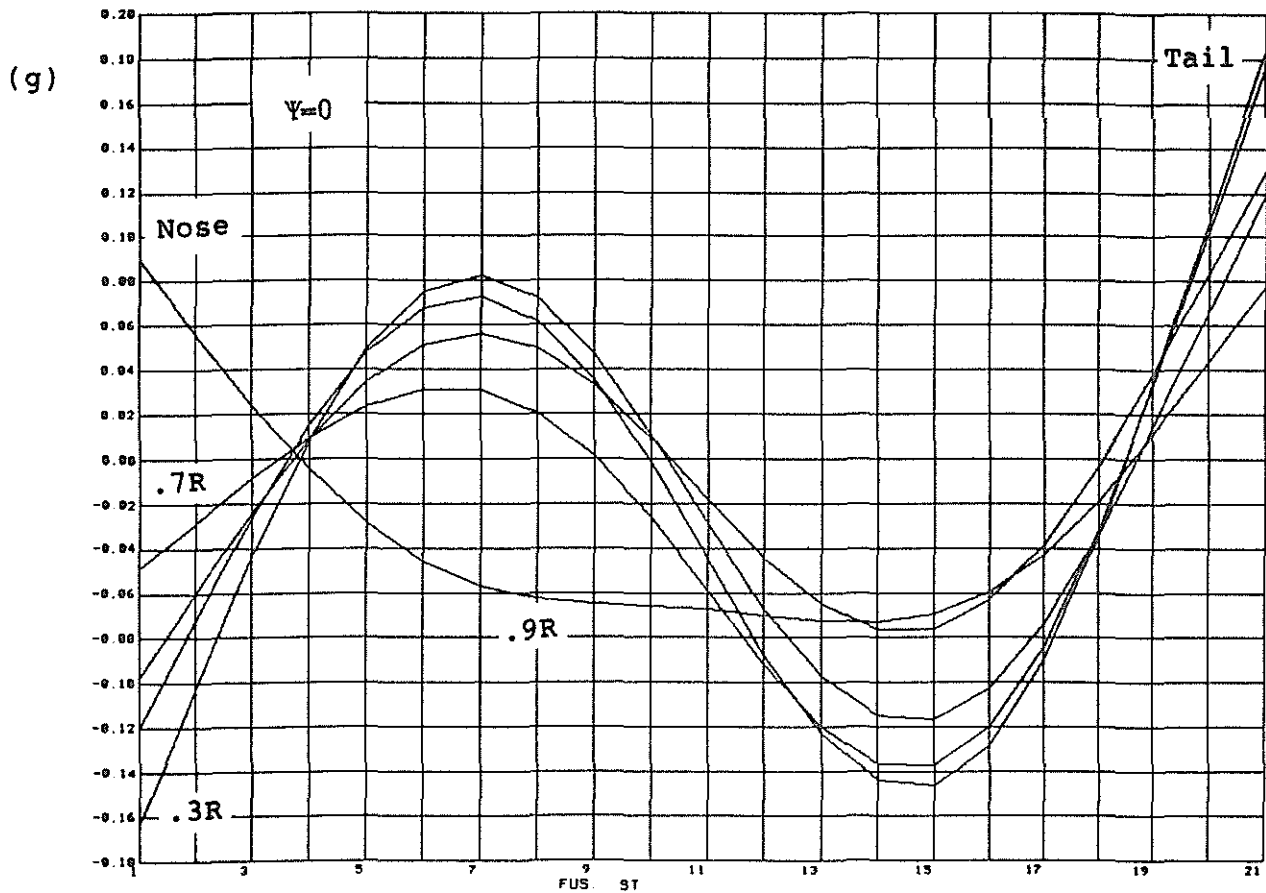
Fig. 8b – Fuselage response for different hub locations
at shi leading blade zero
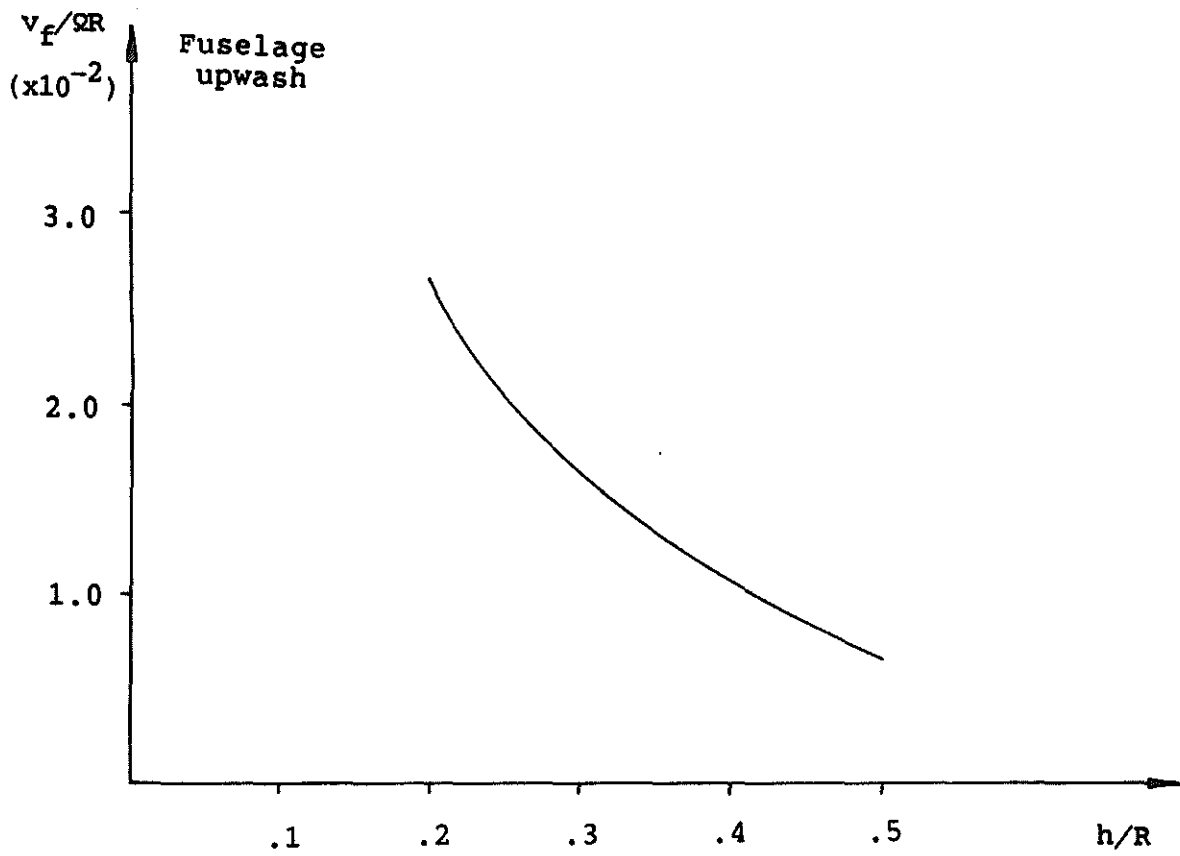
Fig. 9 – Fuselage upwash at
x=0.8 Ψ =180
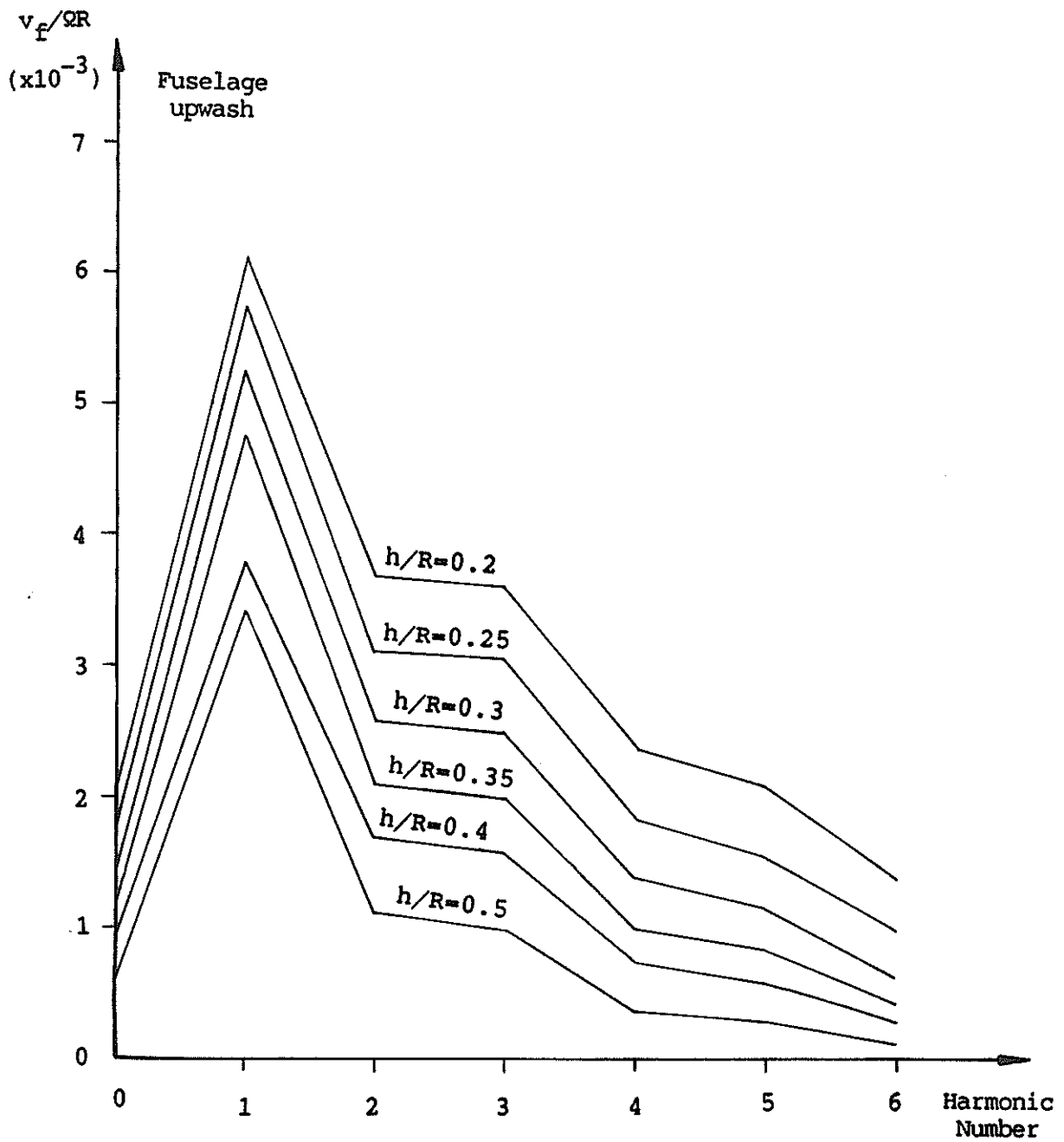
Fig. 10 – Fourier coefficients of upwash at rotor disk
(@ x=0.8 Ψ = 180)
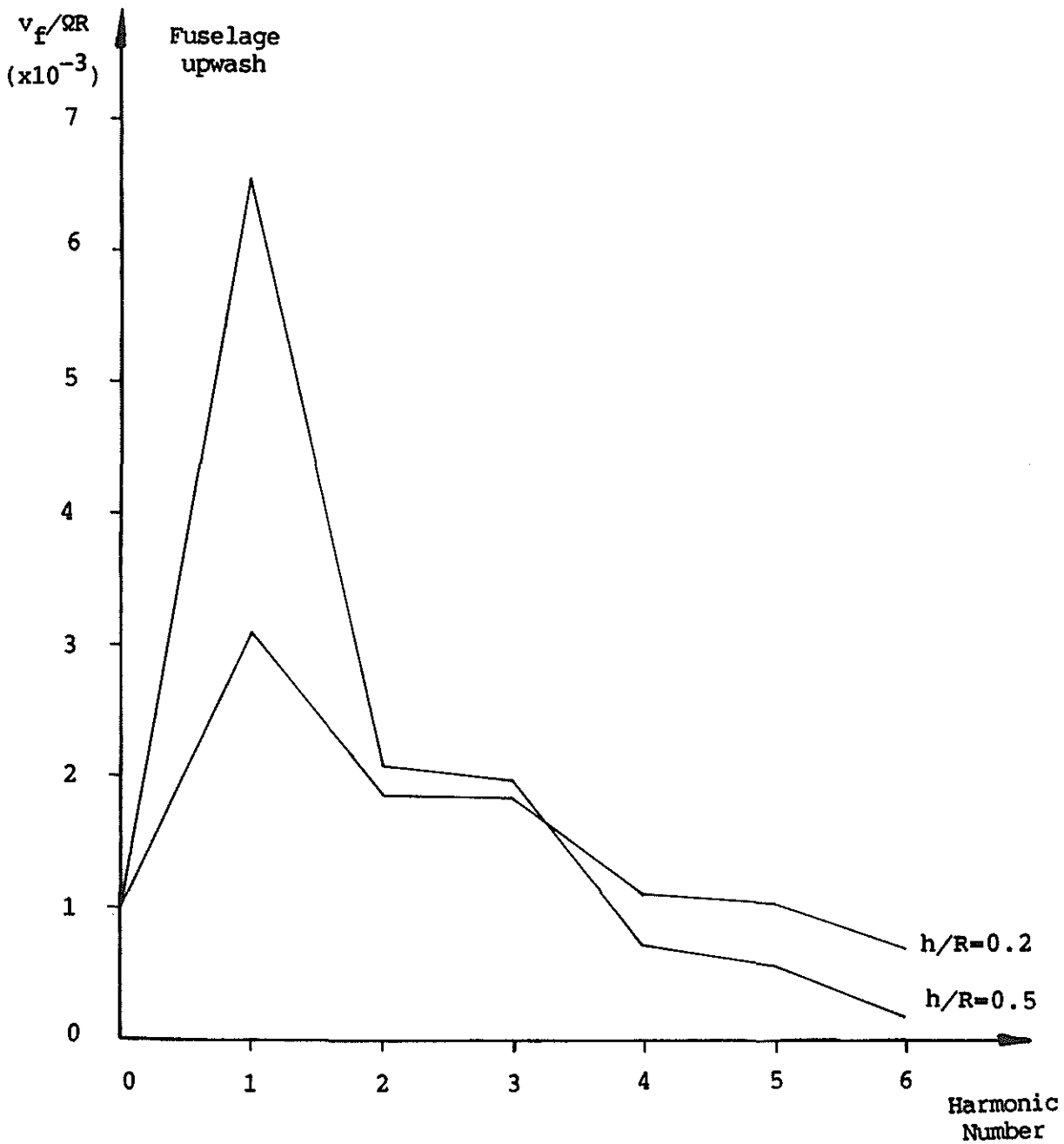
Fig. 11 — Normalized Fourier coefficients
(wrt the constant component)
(@ x=0.8 ψ = 180)

Fuselage
upwash
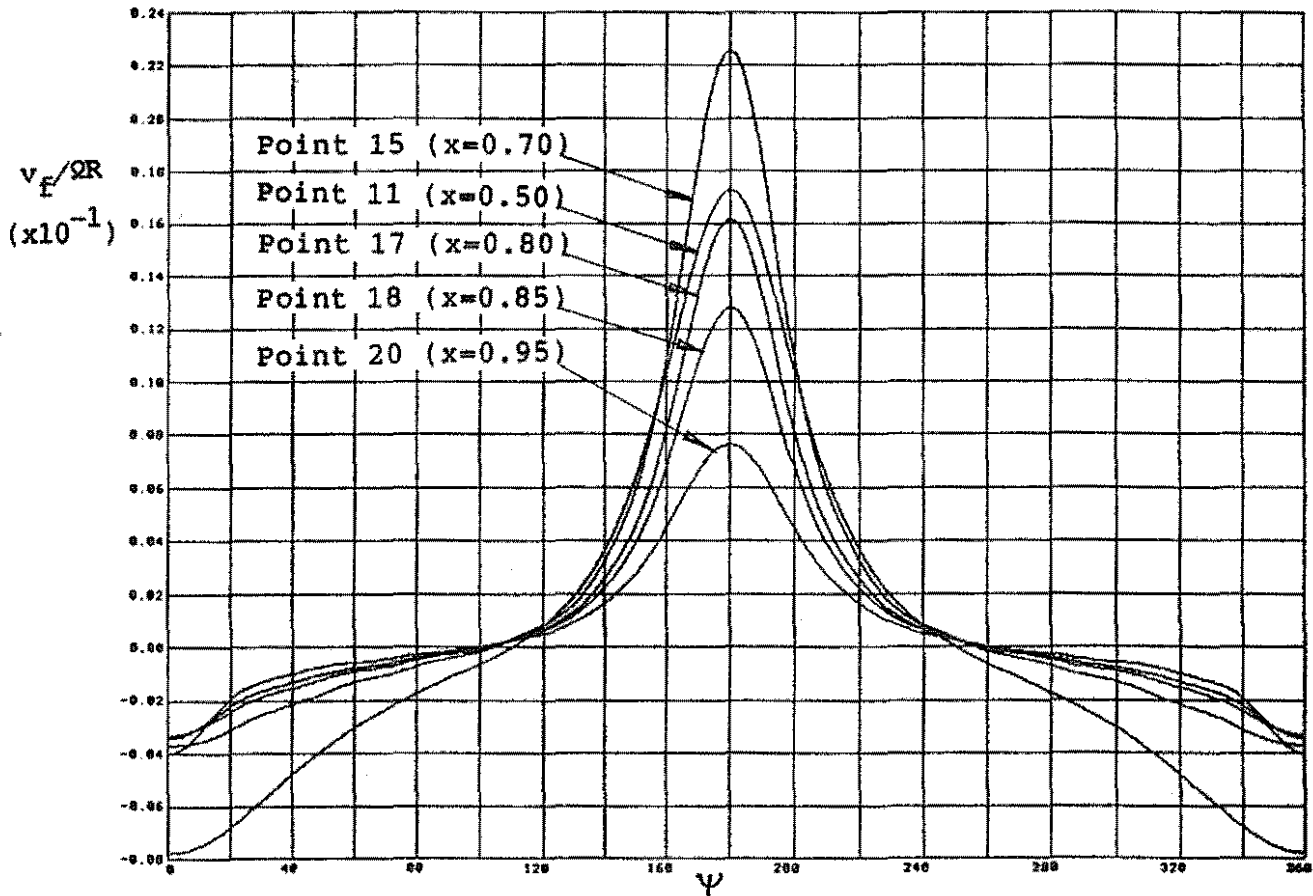
Fig. 12a - Fuselage upwash at different blade locations   h/R=.3
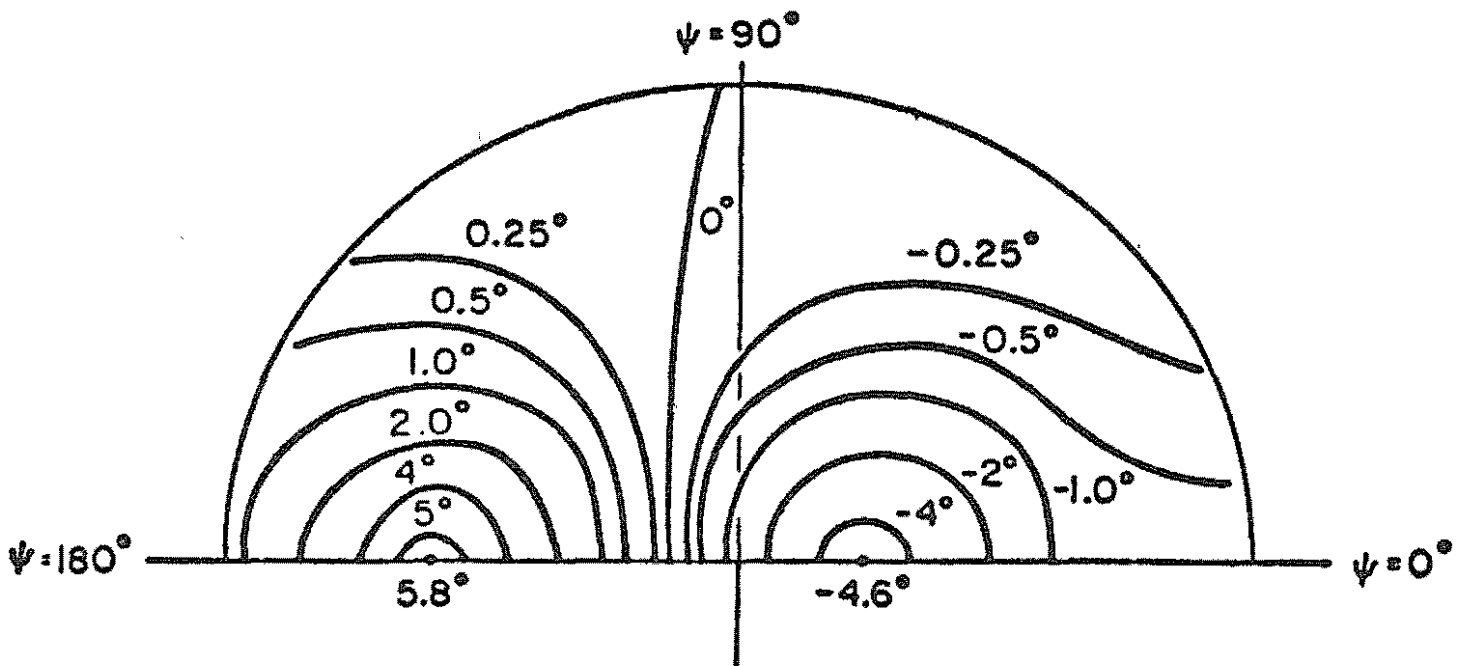
Fig. 12b - Fuselage upwash distribution for basic configuration h/R=.3
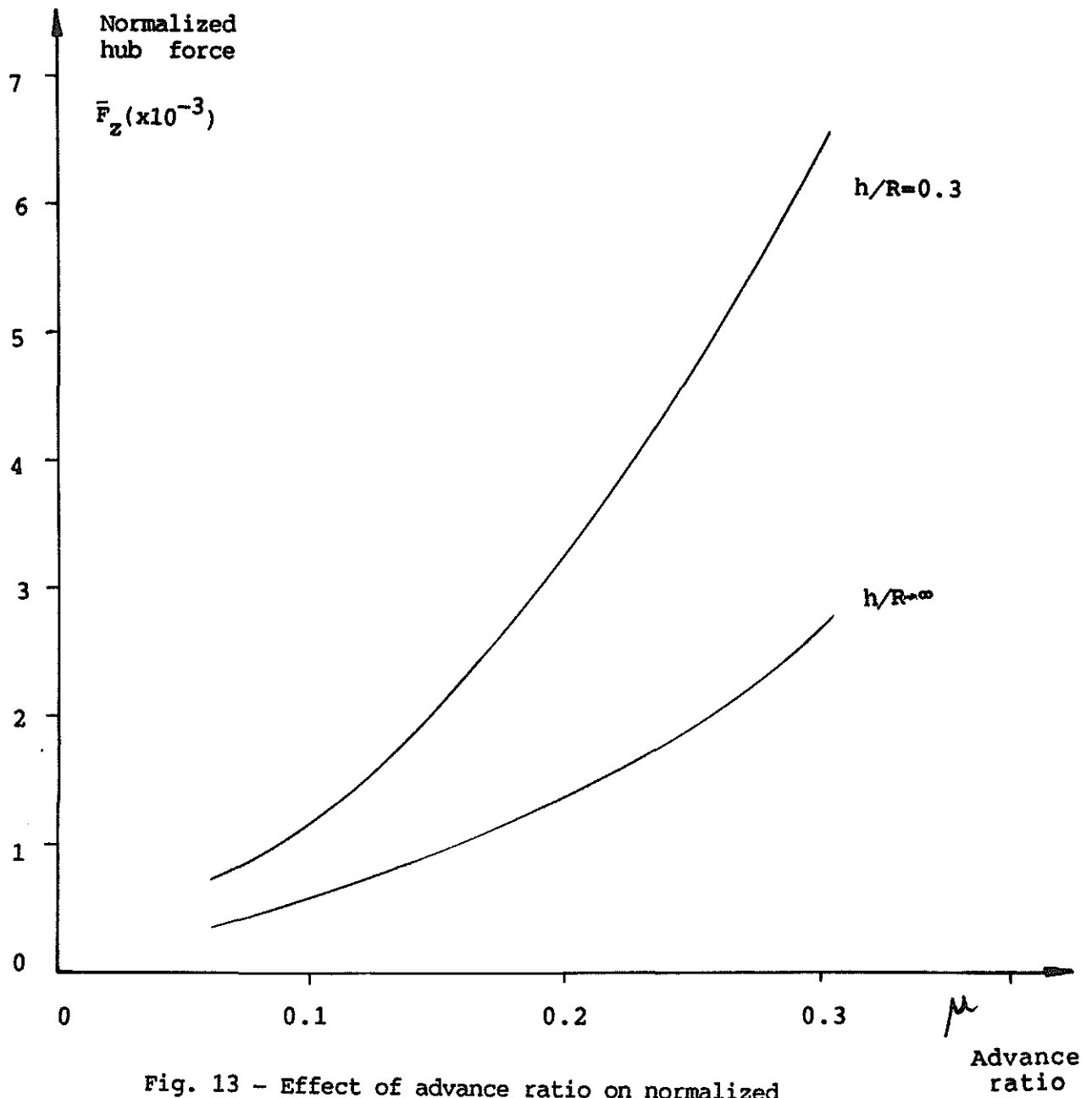
Fig. 13 – Effect of advance ratio on normalized hub force
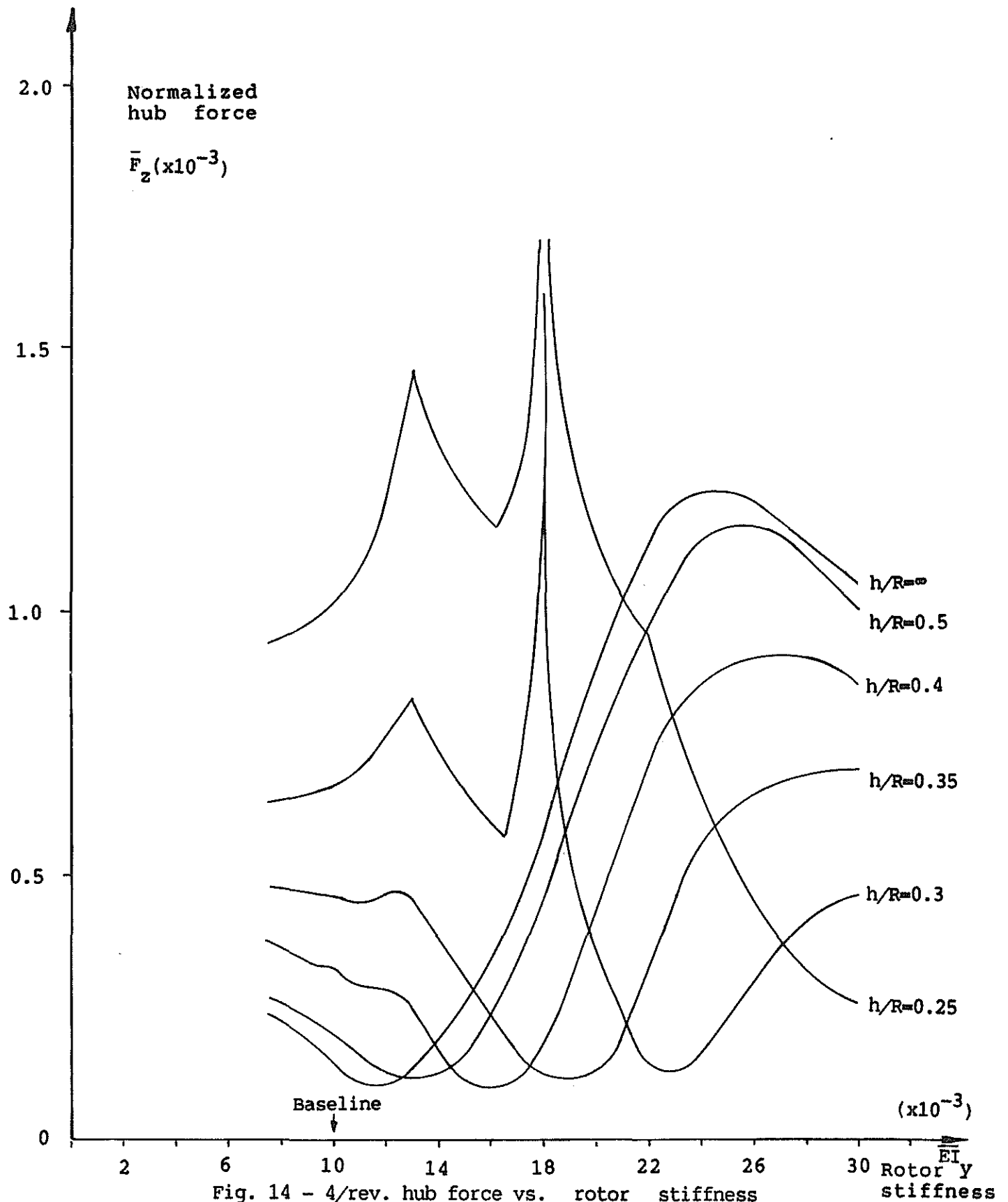
Fig. 14 – 4/rev. hub force vs. rotor stiffness
at different rotor/body clearance
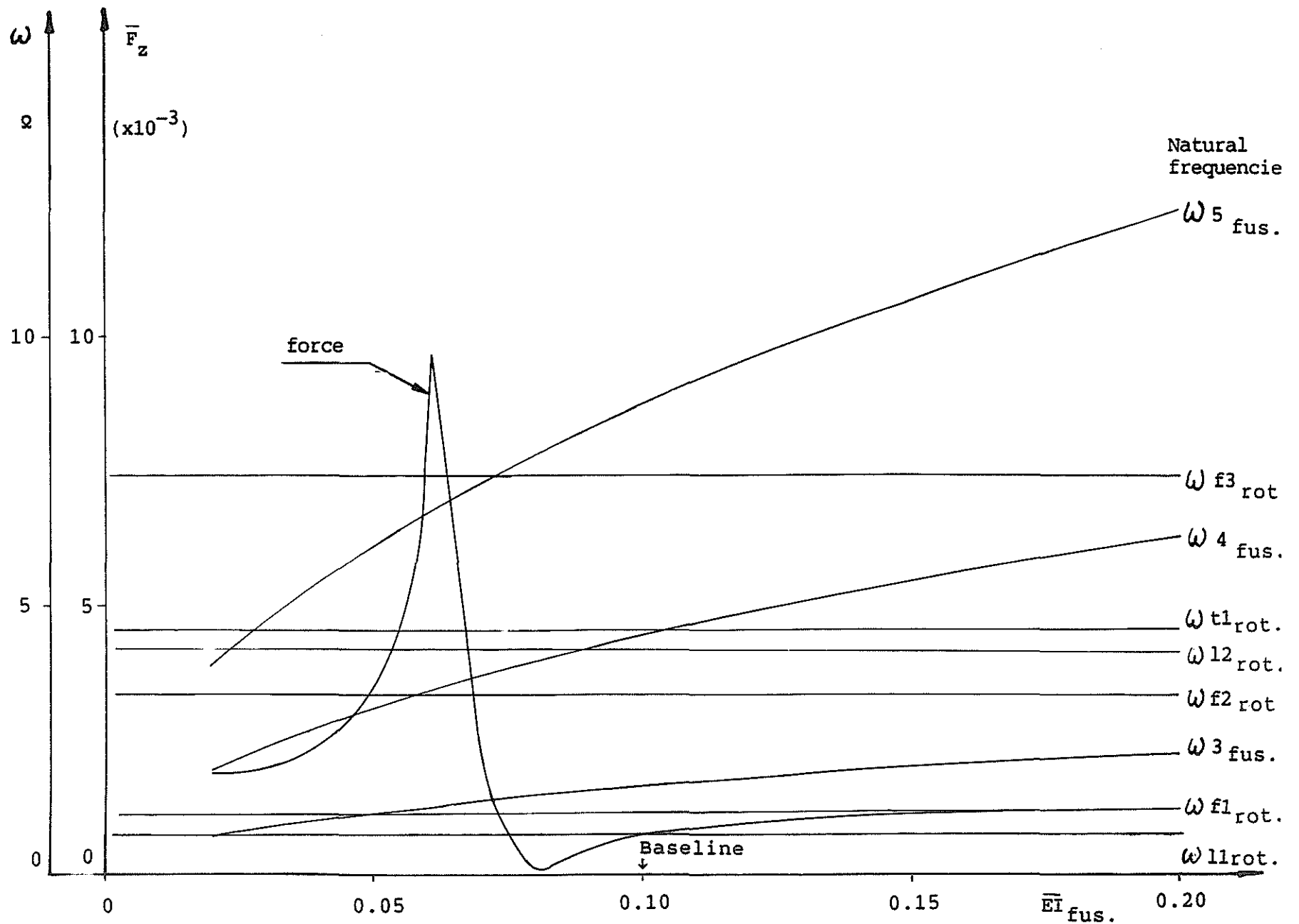
Fig. 15 - Effect of fuselage stiffness on fuselage response